SFN 321 No. 20-29 西合 一矢 (国立天文台)

2019/10/10

20. “Measuring the magnetic field of young stars using iSHELL observations: BP Tau and V347 Aur”
Christian Flores, Michael S. Connelley, Bo Reipurth and Adwin Boogert
21. “Origin of the PN molecule in star-forming regions: the enlarged sample”
F. Fontani, V.M. Rivilla, F.F.S. van der Tak, C. Mininni, M.T. Beltran, and P. Caselli
22. “H2 ortho-para spin conversion on inhomogeneous grain surfaces”
Kenji Furuya, Yuri Aikawa, Tetsuya Hama and Naoki Watanabe
23. “Structure and kinematics of the Taurus star-forming region from Gaia-DR2 and VLBI astrometry”
P.A.B. Galli, L. Loinard, H. Bouy, L. M. Sarro, G.N. Ortiz-Leon, S.A. Dzib, J. Olivares, M. Heyer , J. Hernandez, C. Rom«an-Zuniga, M. Kounkel and K. Covey
24. ”Linking planetesimal and dust content in protoplanetary disks via a local toy model”
Konstantin Gerbig, Christian T. Lenz, and Hubert Klahr
25. ”Chondrule Formation by the Jovian Sweeping Secular Resonance”
Munan Gong, Xiaochen Zheng, Douglas N.C. Lin, Kedron Silsbee, Clement Baruteau, Shude Mao
26. ”Close-in giant-planet formation via in-situ gas accretion and their natal disk properties”
Yasuhiro Hasegawa, Tze Yeung Mathew Yu, and Bradley M. S. Hansen
27. ”How first hydrostatic cores, tidal forces and gravo-turbulent fluctuations set the characteristic mass of stars”
Patrick Hennebelle, Yueh-Ning Lee and Gilles Chabrier
28. ”First sub-arcsecond submillimeter-wave [C I] image of 49 Ceti with ALMA”
Aya E. Higuchi, Kazuya Saigo, Hiroshi Kobayashi, Kazunari Iwasaki, Munetake Momos, Kang Lou Soon, Nami Sakai, Masanobu Kunitomo, Daisuke Ishihara and Satoshi Yamamoto
29. ”L1495 Revisited: A PPMAP View of a Star-Forming Filament”
A.D.P. Howard, A.P. Whitworth, K.A. Marsh, S.D. Clarke, M.J. Griffin, M.W.L. Smith and O.D. Lomax
30. ”Nobeyama 45 m Mapping Observations toward Orion A. II. Classification of cloud structures and variation of the 13CO/C18O abundance ratio due to far-UV Radiation”
Shun Ishii, Fumitaka Nakamura, Yoshito Shimajiri, Ryohei Kawabe, Takashi Tsukagoshi, Kazuhito Dobashi, Tomomi Shimoikura

Structure and kinematics of the Taurus star-forming region from Gaia-DR2 and VLBI astrometry

P.A.B. Galli, L. Loinard, H. Bouy, L. M. Sarro, G.N. Ortiz-Leon, S.A. Dzib, J. Olivares, M. Heyer,
J. Hernandez, C. Roman-Zuniga, M. Kounkel and K. Covey

Accepted by A&A https://arxiv.org/pdf/1909.01118.pdf

おうし座星形成分子雲に付随する若い星の運動・距離構造をGaia space mission DR2とVLBIの最新の結果を用いて調べ、それらが21個のクラスター構造に分けられること、極めて分子ガスとの視線速度の相関が良いことを示した。

<u>サンプル</u>

- 牡牛座分子雲領域
- Gaia space mission DR2（第2回data release)、またはVLBIカタログ
- 若い< 10Myの星 (2MASSカタログとcross-match)

=> 411 stars（うち、精度よく値が決まっている 248stars を解析に使用）
精度: parallaxes 0.1 mas以上、proper motion 0.1 mas/yr 以上

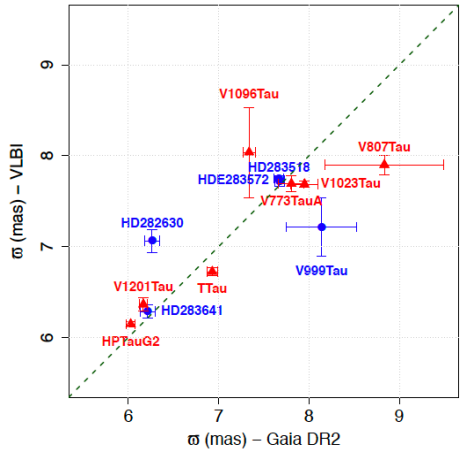

Fig1. Gaia DR2とVLBI (GOBELINS project)の年周視差 ϖ (mas)の相関。 青はsingle star, 赤はbinary

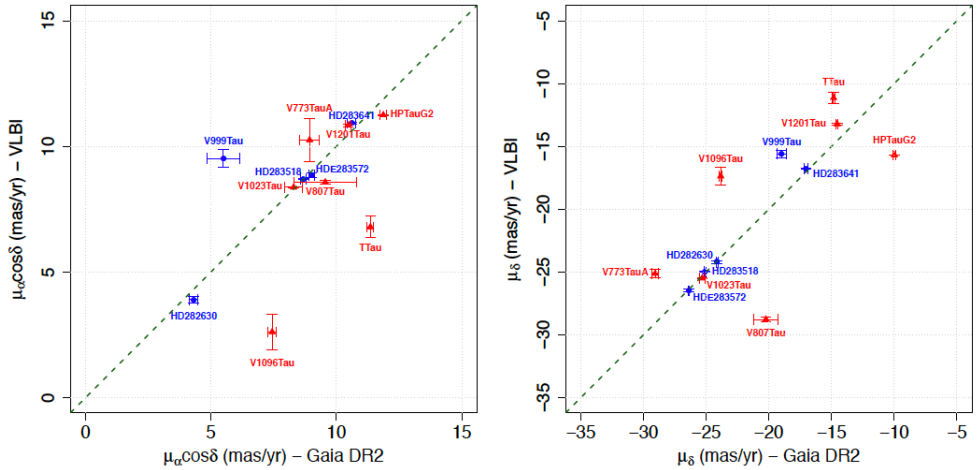

Fig2. Gaia DR2とVLBI (GOBELINS project)の固有運動(mas/yr)の相関。 青はsingle star, 赤はbinary

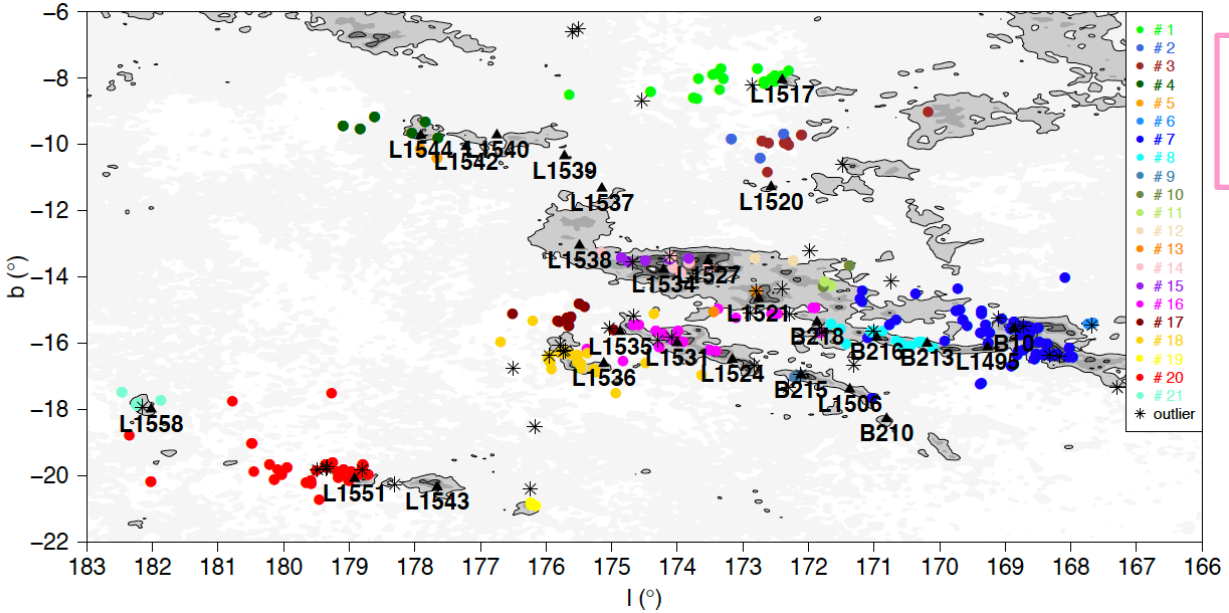

284 starsの年周視差と固有運動を階層的クラスター解析(HMAC) => 21 clustersになった。

L1495 (cluster#7)とB213 - B216 (cluster #8) は空間的には近いが距離が異なるためにcluster解析では異なる幹にある(下のマゼンタで囲った)。

Fig.4 284の星の空間分布 +AV map (Dobashi et al. 2005)

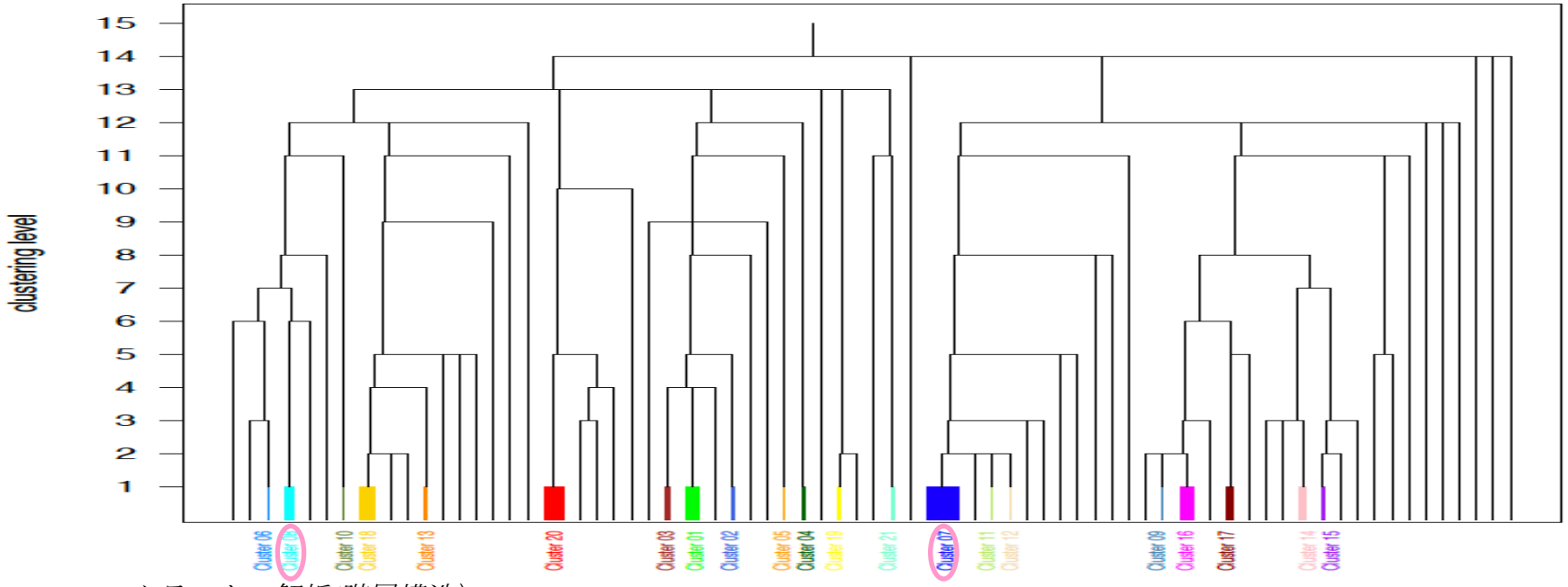

Fig. 3 クラスター解析(階層構造)

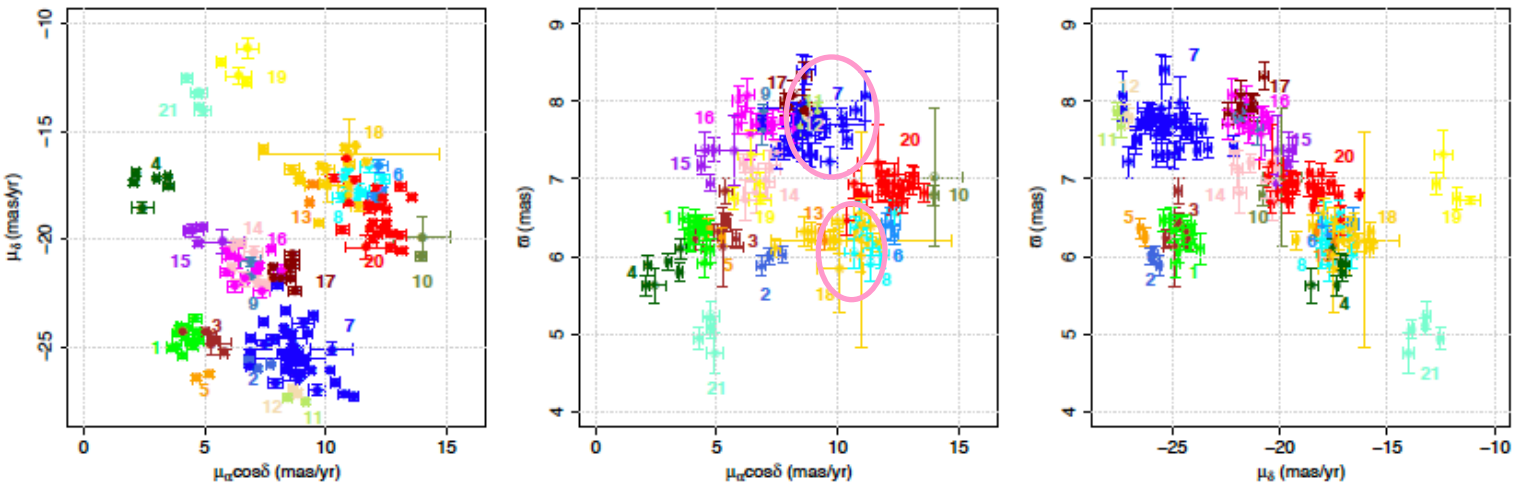

Fig. 5 各クラスターの年周視差・固有運動分布

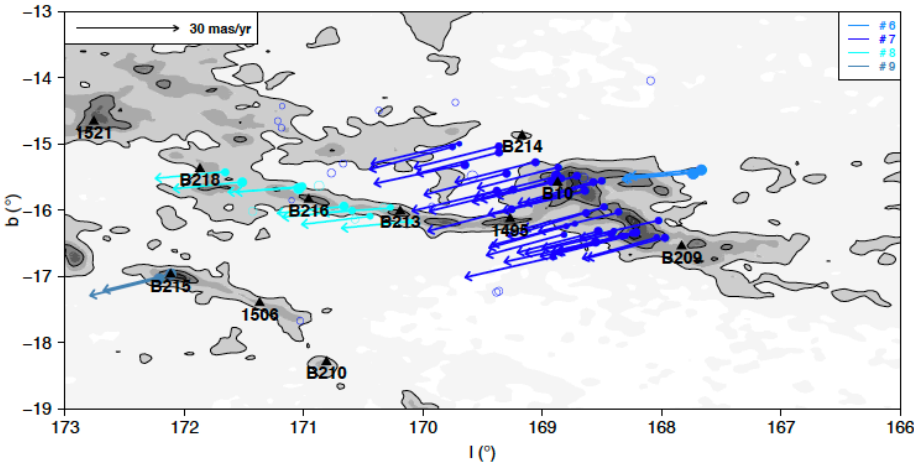

Fig. 7 L1495 (cluster#7)とB213 - B216 (cluster #8) 領域

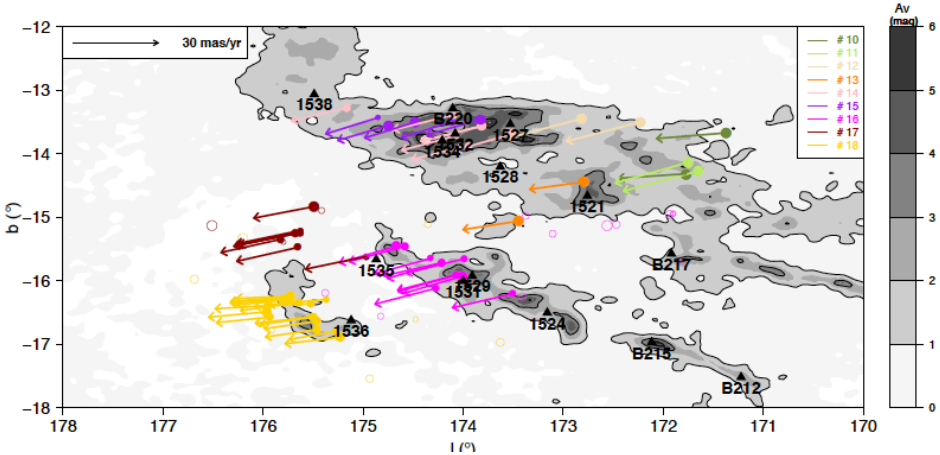

Fig. 8 Heiles Cloud 2領域 cluster #10 - #18

Heiles Cloud 2領域 にあるCluster #14 とCluster #15は空間的にはover lapしているが、運動が少し異なるクラスターとして認識される。

Skip (参考)

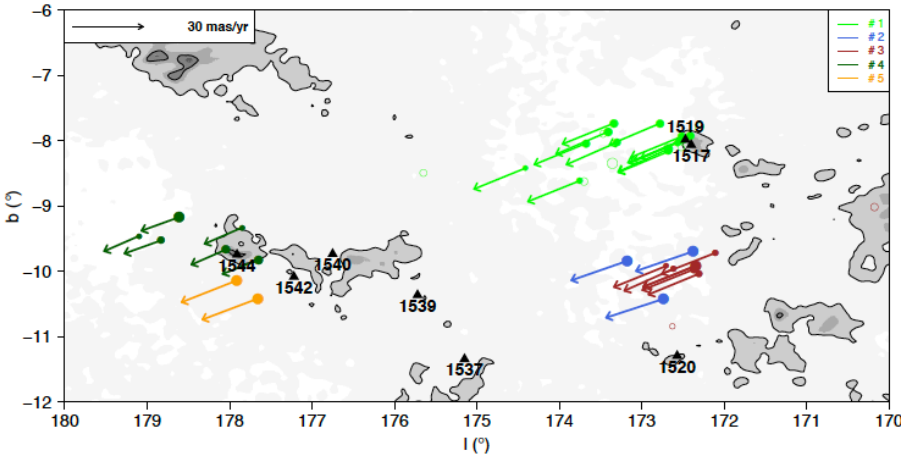

Fig. 6 Cluster#1 - #5 領域

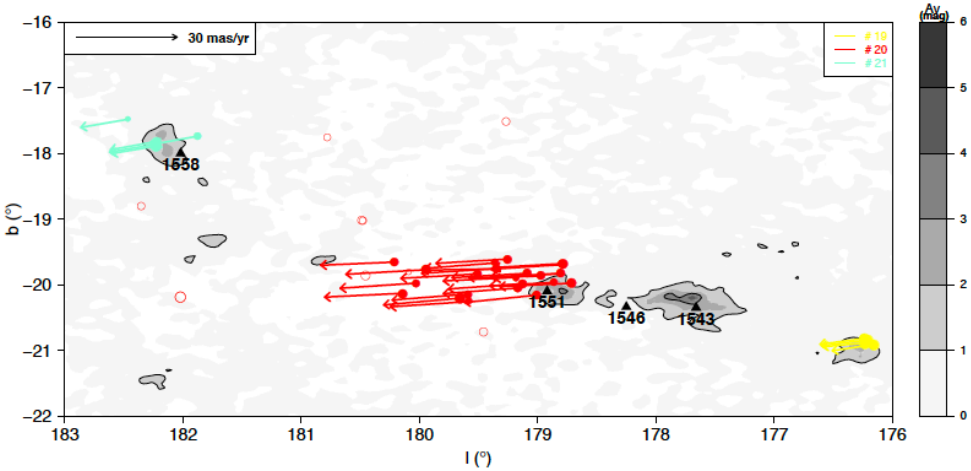

Fig. 8 Cluster#19 - #21 領域

Table 3. Properties of the clusters obtained with HMAC.

Cluster	N_0	N	α (h:m:s)	δ (° ′ ″)	l (deg)	b (deg)	$\mu_\alpha \cos\delta$ (mas/yr)			μ_δ (mas/yr)			ϖ (mas)			Molecular Clouds
							Mean ± SEM	Median	SD	Mean ± SEM	Median	SD	Mean ± SEM	Median	SD	
1	21	14	04:57:04.1	30:05:31	173.0	-8.0	4.249 ± 0.095	4.247	0.356	−24.578 ± 0.125	-24.644	0.470	6.281 ± 0.045	6.325	0.167	L 1517, L 1519
2	3	3	04:49:17.7	29:05:52	172.8	-10.0	7.249 ± 0.262	7.185	0.453	−25.814 ± 0.117	-25.800	0.203	5.965 ± 0.045	5.998	0.078	
3	9	7	04:48:29.6	29:25:15	172.4	-9.9	5.187 ± 0.200	5.336	0.529	−24.701 ± 0.126	-24.732	0.334	6.369 ± 0.089	6.316	0.236	
4	6	6	05:06:04.2	25:01:35	178.3	-9.5	2.773 ± 0.263	2.709	0.645	−17.435 ± 0.237	-17.273	0.580	5.825 ± 0.076	5.842	0.185	L 1544
5	2	2	05:01:50.5	25:00:37	177.8	-10.3	4.923 ± 0.112	4.923	0.522	−26.374 ± 0.085	-26.374	0.214	6.304 ± 0.087	6.304	0.104	
6	3	3	04:15:42.3	29:11:41	167.7	-15.4	12.173 ± 0.097	12.183	0.168	−17.458 ± 0.436	-17.754	0.755	6.365 ± 0.042	6.397	0.073	L 1495 NW
7	54	39	04:17:16.9	28:08:55	168.7	-15.9	8.704 ± 0.157	8.614	0.981	−25.308 ± 0.179	-25.347	1.116	7.673 ± 0.037	7.692	0.233	L 1495
8	13	9	04:23:36.1	26:44:03	170.8	-15.8	11.255 ± 0.180	11.196	0.541	−17.482 ± 0.184	-17.730	0.552	6.223 ± 0.072	6.235	0.215	B 213, B 216
9	2	2	04:23:37.3	24:59:38	172.2	-17.0	6.907 ± 0.209	6.907	0.023	−21.362 ± 0.129	-21.362	0.672	7.741 ± 0.106	7.741	0.226	B 215
10	2	2	04:31:57.7	27:24:45	171.6	-14.0	13.973 ± 0.602	13.973	0.030	−20.344 ± 0.469	-20.344	0.906	6.903 ± 0.452	6.903	0.231	
11	2	2	04:31:36.8	27:10:48	171.7	-14.2	8.803 ± 0.123	8.803	0.736	−27.480 ± 0.105	-27.480	0.191	7.780 ± 0.089	7.780	0.189	
12	2	2	04:36:26.7	27:03:04	172.5	-13.5	8.743 ± 0.133	8.743	0.218	−27.082 ± 0.100	-27.082	0.186	7.820 ± 0.086	7.820	0.069	
13	2	2	04:33:46.9	25:47:03	173.1	-14.7	9.397 ± 0.119	9.397	0.135	−17.878 ± 0.093	-17.878	0.825	6.255 ± 0.084	6.255	0.103	
14	9	7	04:40:22.3	25:50:19	174.1	-13.6	6.728 ± 0.194	6.628	0.514	−21.195 ± 0.310	-21.340	0.820	7.046 ± 0.081	7.122	0.215	Heiles Cloud 2: L 1527, L 1532, L 1534, B 220
15	5	5	04:41:38.0	25:38:26	174.4	-13.5	4.847 ± 0.237	4.727	0.529	−19.799 ± 0.155	-19.630	0.347	7.247 ± 0.084	7.366	0.188	Heiles Cloud 2: L 1527, L 1532, L 1534, B 220
16	23	11	04:33:12.4	24:19:57	174.2	-15.8	6.799 ± 0.236	6.651	0.783	−21.353 ± 0.194	-21.444	0.642	7.768 ± 0.046	7.710	0.152	L 1535, L 1529, L 1531, L 1524
17	11	8	04:38:42.0	23:38:14	175.6	-15.3	8.368 ± 0.131	8.548	0.370	−21.556 ± 0.182	-21.570	0.516	7.984 ± 0.057	7.943	0.161	
18	24	17	04:34:50.4	22:49:58	175.6	-16.5	10.146 ± 0.280	10.082	1.156	−16.994 ± 0.238	-16.770	0.979	6.243 ± 0.042	6.212	0.171	L 1536
19	4	4	04:22:00.2	19:33:57	176.2	-20.9	6.416 ± 0.253	6.586	0.506	−12.006 ± 0.355	-12.082	0.711	6.932 ± 0.136	6.845	0.272	T Tau cloud
20	34	24	04:32:59.4	17:57:15	179.3	-19.9	12.068 ± 0.168	12.118	0.822	−18.846 ± 0.236	-18.943	1.157	6.880 ± 0.032	6.908	0.158	L 1551
21	5	5	04:47:09.1	17:05:31	182.2	-17.8	4.686 ± 0.114	4.757	0.255	−13.375 ± 0.269	-13.254	0.602	5.015 ± 0.081	5.058	0.180	L 1558

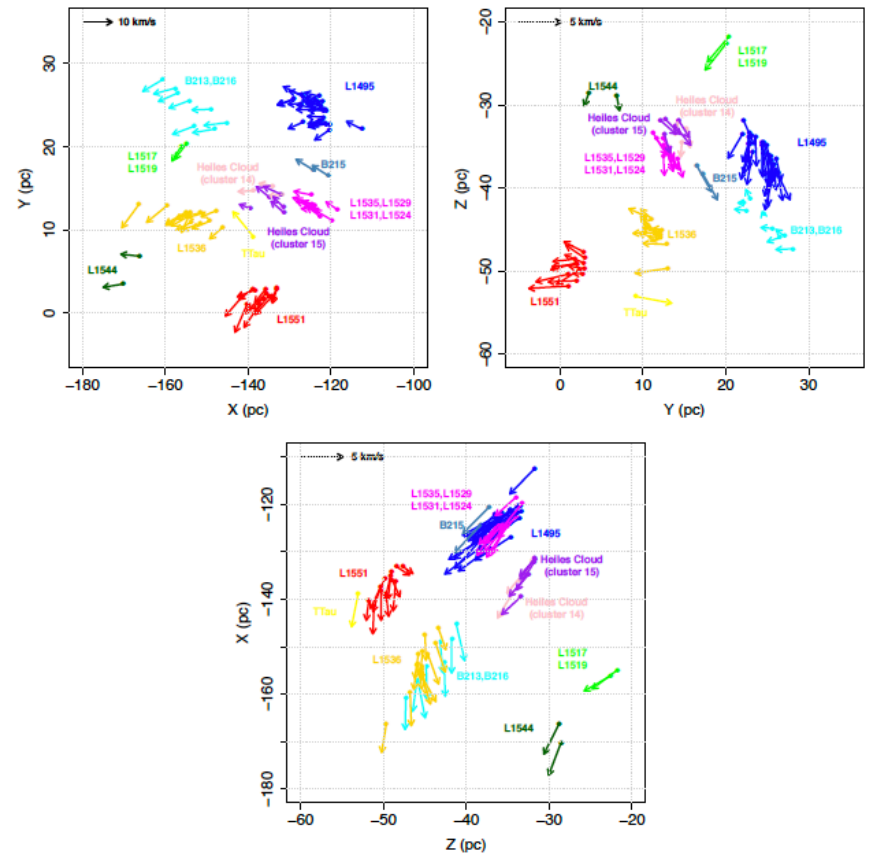

Fig. 13. Peculiar velocity of the stars in the various clouds of the Taurus complex projected onto the XY, YZ, and ZX planes.

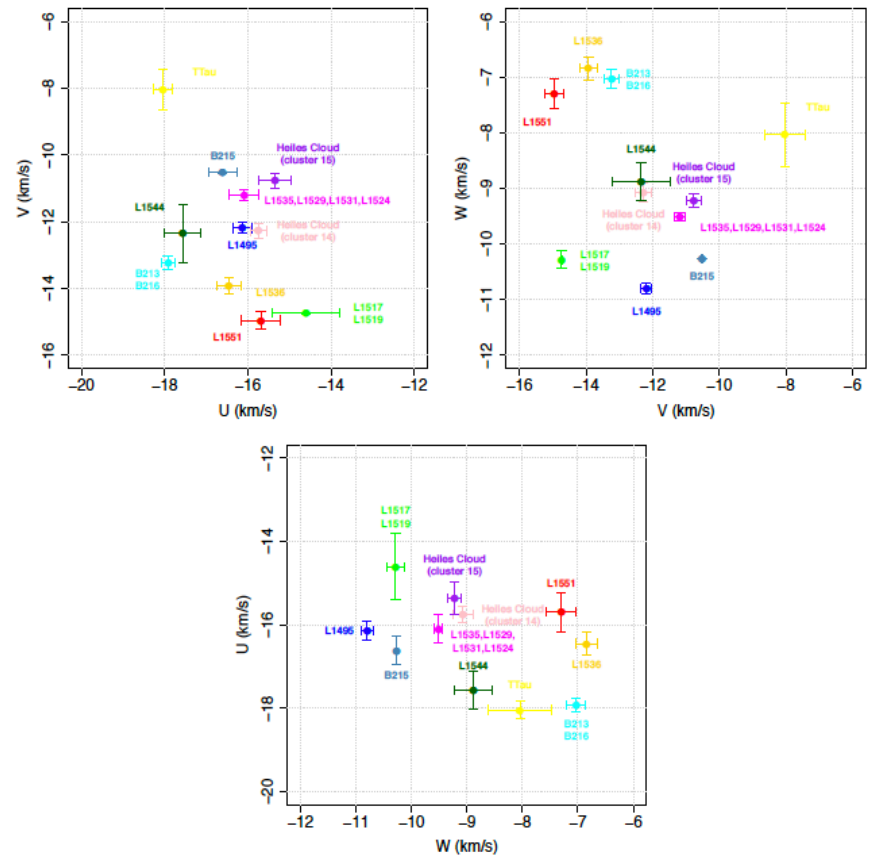

Fig. 14. Mean spatial velocity of the stars projected towards the various molecular clouds of the Taurus complex.

全体の内部運動の解析

- 牡牛座全体でのExpansion (contraction) 速度は見られない0.0 ± 0.1 km/s。
  ⇔ radial motionはランダム運動に起因。
- Rotation 速度が存在 1.5 ± 0.1 km/s (ただし全体の速度分散2.7km/sに比べたら小さい)

クラスターの間の距離は4pc ～50pc (平均25pcでありこれはcrossing time 数Myrに相当)

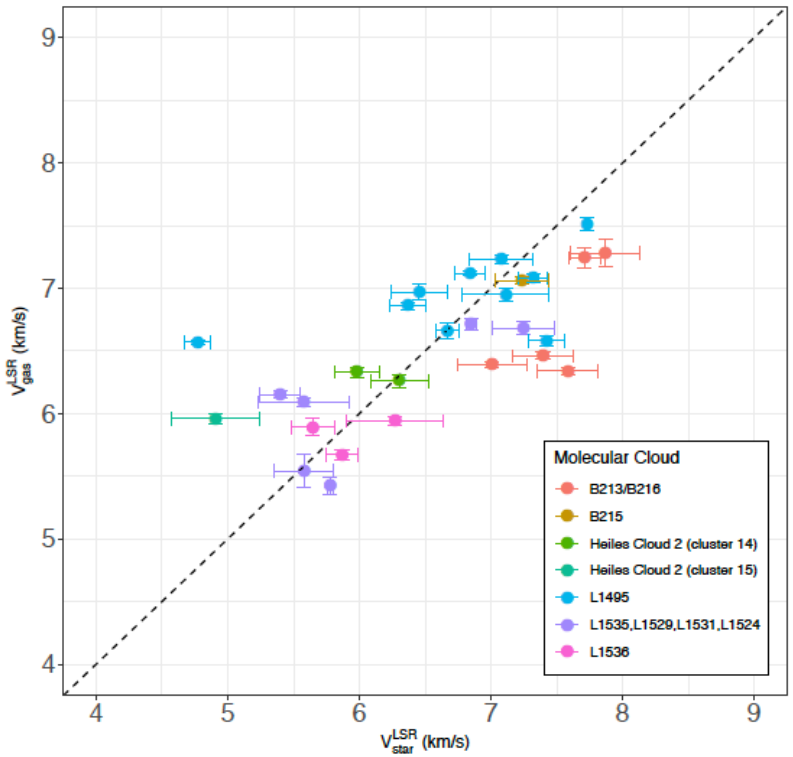

Fig. 15. Comparison of the radial velocity of the stars (with respect to the LSR) with the centroid velocity of the ^{13}CO emission extracted from the FCRAO maps at the position of each star. The black dashed line indicates a perfect correlation between the two measurements, and the colors respresent the various molecular clouds to which the stars belong.

若い星たちとcloudの視線速度は良い相関を示す

How first hydrostatic cores, tidal forces and gravo-turbulent fluctuations set the characteristic mass of stars

Patrick Hennebelle, Yueh-Ning Lee and Gilles Chabrier

Accepted by ApJ http://arxiv.org/pdf/1908.07250

３次元高解像度シミュレーション(ARM, MHD)を用いて、IMFが、dustのopacity limitや潮汐力などの局所プロセスで決まるというアイデアをテストした(つまり、最終質量が最も近い分裂片により決定されるというアイデア)。結果は、質量関数のピークがFirst Adiabatic Core質量のおよそ数倍～10倍の場所に現れるという局所プロセスによる質量決定を裏付けるものであった。

計算

- ３次元MHDシミュレーション (AMRで最大4au解像度) + sink particle (10^{11} cm^{-3}で導入)
- barotropic状態方程式(輻射輸送計算の結果を近似)

$$T = T_0 \left\{ 1 + \frac{(n/n_{\rm ad})^{(\gamma_1 - 1)}}{1 + (n/n_{\rm ad,2})^{(\gamma_1 - \gamma_2)}} \right\},$$

ただし、T_0 = 10K, $n_{ad} = 10^{10}$ cm^{-3}, $n_{ad;2} = 3 \times 10^{11}$cm^{-3}, $\gamma_1 = 5/3$, $\gamma_2 = 7/5$.
=> FHSC (first Hydrostatic Core)は $M \sim 0.02$~$0.03 M_\odot$, $R \sim 15$ auとなる。

- ２つの Model (どちらも全ガス質量 = 1000$M_\odot$)
  - Run1: 孤立 spherical gas clump。
    初期乱流は速度分散~2km/s (Mach 10)。
    $R \sim 0.1$pc ($n \sim 5 \times 10^6$ cm^{-3})
  - Run 2: 周期境界。
    k = 1-3乱流(Mach 10に相当)。
    $R \sim 0.5$pc ($n \sim 10^6$ cm^{-3})

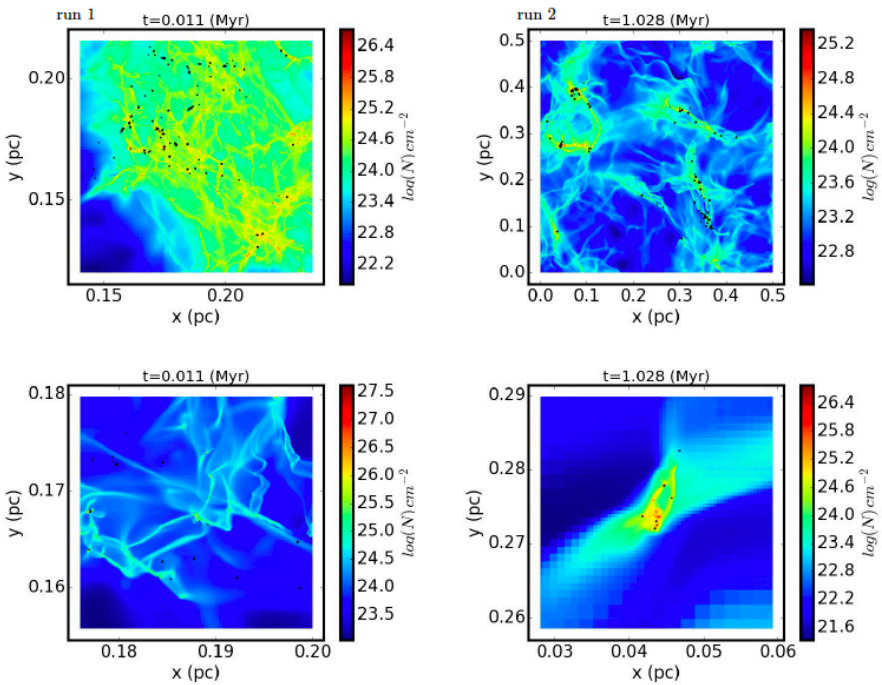

Figure 1. Column density of run1 (left) and run2 (right). Top panels show most of the whole cloud while bottom panels represent zoomed regions. The black dots represent the sink particles aiming to model the stars.

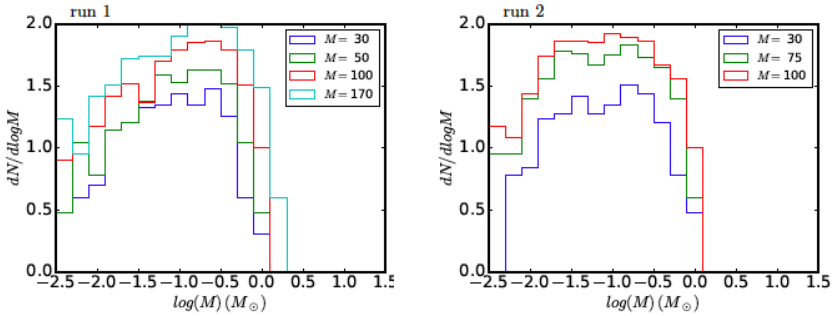

Fig. 2 Run 1, Run2の質量関数の時間進化(Mは降着ガス質量 M⊙)
生成された全sink particle数はそれぞれ762と723個。

つまり、Mass peak = 0.1-0.2M⊙、質量関数のベキ～$M^{-0.75}$
これは過去の研究と一致(paper I, II)

付近(140au, 240au)に他のparticleがあるときは生成しないというテスト

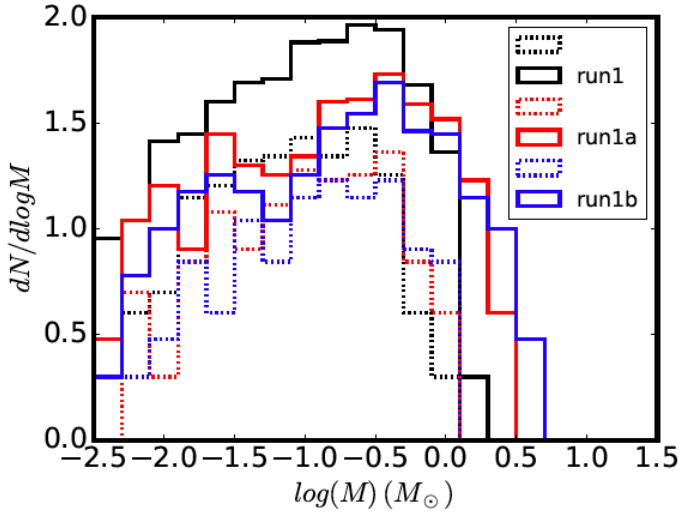

Fig. 4 sink particle生成の基準を変更
(実線 M=150M⊙, 点線 M =50M⊙)

近くでのsink生成を手で止めると質量peakが大きくなる
(1 制限なし、1a 140au 以内, 1b 240以内でのsink生成禁止)。

=> 最も近い分裂片が質量降着を妨げることで質量(ピーク)が大きくなることをデモンストレートしている。

=> 質量関数の決定メカニズは知るには、最も近い分裂を起こしている物理状態を明らかにする必要がある。

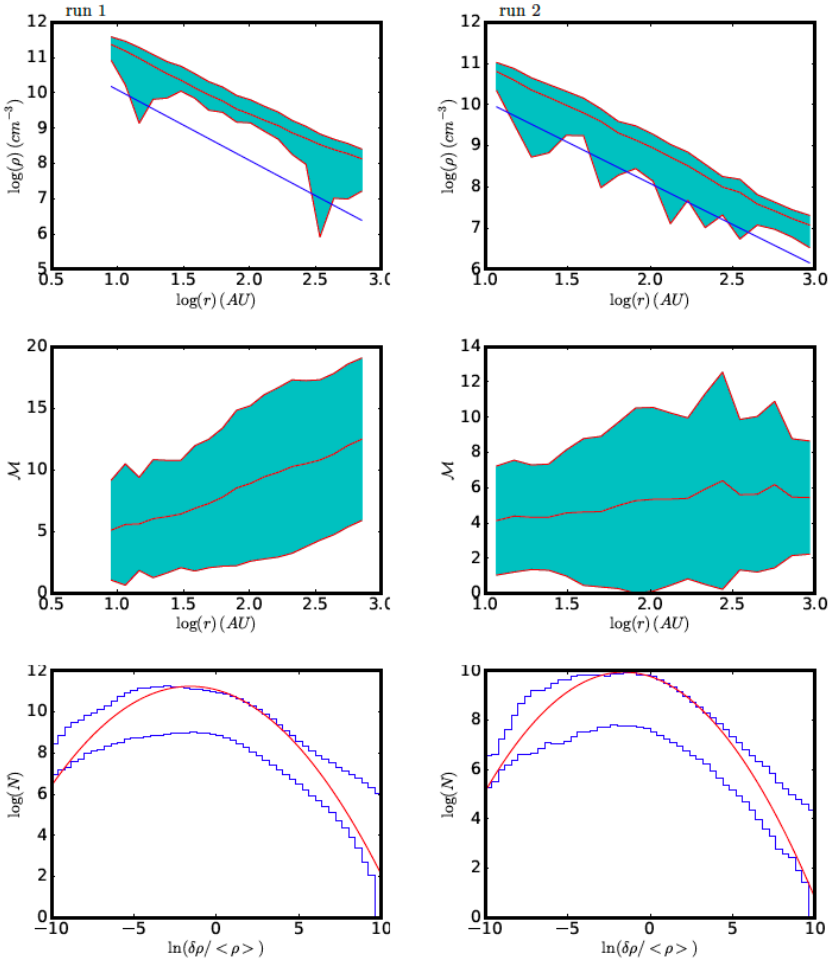

Figure 5. Gas statistics around the sinks younger than 1000 yr. Left: run1, right: run2. Top panels show the mean density (red line) and the mean standard deviation (blue shaded area). For reference, the blue line shows the density of the singular isothermal sphere, $n_{SIS} = \rho_{SIS}/m_p$. We see that on average the density is about $10 \times \rho_{SIS}$ for run1 and about $7 \times \rho_{SIS}$ for run2. Middle panels display the mean Mach numbers, which below 300 AU is found to be about 5-10 for run1 and 4-5 for run2. Bottom panels portray the distribution of the density fluctuations (i.e. with respect to the mean density shown on top panel) within a sphere of radius 800 AU (upper curve) and 250 AU (lower curve). For reference the red curves represent a log-normal distribution with a width $\sigma^2 = \ln(1 + b^2\mathcal{M}^2)$ with $b = 0.8$ and $\mathcal{M} = 6$.

Age = 1000yrにおけるsink周辺の物理状態（緑は1σ分布）

- Top panel : 平均密度分布
  Singular Isothermal Sphere(青線）の7-10倍の係数のr^{-2}ベキ分布
- Middle panel: Mach数
- Bottom panel: Density PDF
  2つの青線は<800au、<240auでのPDF。
  赤はlognormal($\sigma^2 = \ln[1 + b^2 M^2]$ただし、$M$=6, b=0.8。

<u>解析的理解 （雰囲気だけ、、）</u>

- 密度がSISの係数分布であるのでenvelopeは

$$M_{env}(r) = \int \rho_{env}(r) 4\pi r^2 dr = 2A\frac{c_s^2}{G} r = M_L \tilde{r},$$

ただし、A~10、M_Lはmass limit でr~はその半径。

- エンベロープの密度揺らぎは1 σ分布から以下のように近似

$$P(\tilde{r}, \delta_\rho(\tilde{r})) = \frac{1}{\sqrt{2\pi}\sigma(\tilde{r})} \exp\left[\frac{-\left(\delta_\rho(\tilde{r}) + \sigma^2(\tilde{r})/2\right)^2}{2\sigma^2(\tilde{r})}\right],$$

- PDFの結果から局所乱流(Mach数）は、

$$\mathcal{M}(\tilde{r}) = \frac{1}{c_s}\sqrt{\epsilon \frac{G[M_L + M_{env}(r)]}{r}} = \sqrt{2A(1 + \frac{1}{\tilde{r}})\epsilon}.$$ ここでε~1

こんな感じでモデル化を行いビリアルを使ってエンベロープの自己重力不安定を調べると、その分裂がその後の成長を抑制し最終的な星の質量が決まることを確認できる。

$$E_{vir}(r_n, \delta r_n, n_n) = E_g(r_n, \delta r_n, n_n) + 2E_{ther} + 2E_{kin} - VP_{ext} - VP_{ram}$$

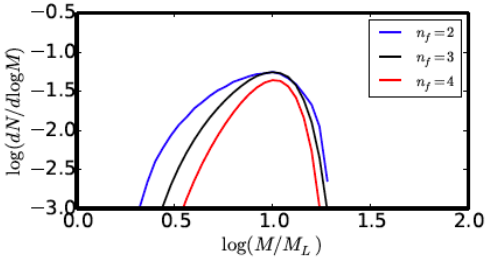

First sub-arcsecond submillimeter-wave [C I] image of 49 Ceti with ALMA

Aya E. Higuchi, Kazuya Saigo, Hiroshi Kobayashi, Kazunari Iwasaki, Munetake Momos, Kang Lou Soon, Nami Sakai, Masanobu Kunitomo, Daisuke Ishihara and Satoshi Yamamoto

Accepted by ApJ https://arxiv.org/pdf/1908.07032

49 CetiのDebris disks のALMA Band 8観測による[C I] $^3P_1$–$^3P_0$ emission観測。過去のCO(3-2)観測と比較すると、[C I]/CO(J=3–2)比が円盤外縁部で高くなってることがわかった。これはinterstellar UV radiation fiがCO乖離を起こしている結果と思われる。

49 Ceti

- 近傍(d = 57±0.3 pc)のほぼedge-on debris disks を持つA型星
- 年齢 = 12 – 50 Myr、星質量 = 2.1 $M_\odot$
- 半径~100auのリング状のダスト・CO分布 （過去のALMA観測）

過去のASTE 10 m観測にて[C I] $^3P_1$–$^3P_0$ emissionが検出されている。そのCOとline profileが似ているため、COとCが共存していると思われるが、空間分解できていない。

今回、ALMAにより、詳細なCIの分布を観測しCOと比較した。

Fig1. 49 CetiのALMA観測結果
(a)今回のBand 8ダスト連続波イメージ、
(b) 今回のBand 8 [CI]イメージ、
(c) 過去のALMA観測のCO mom 0 map

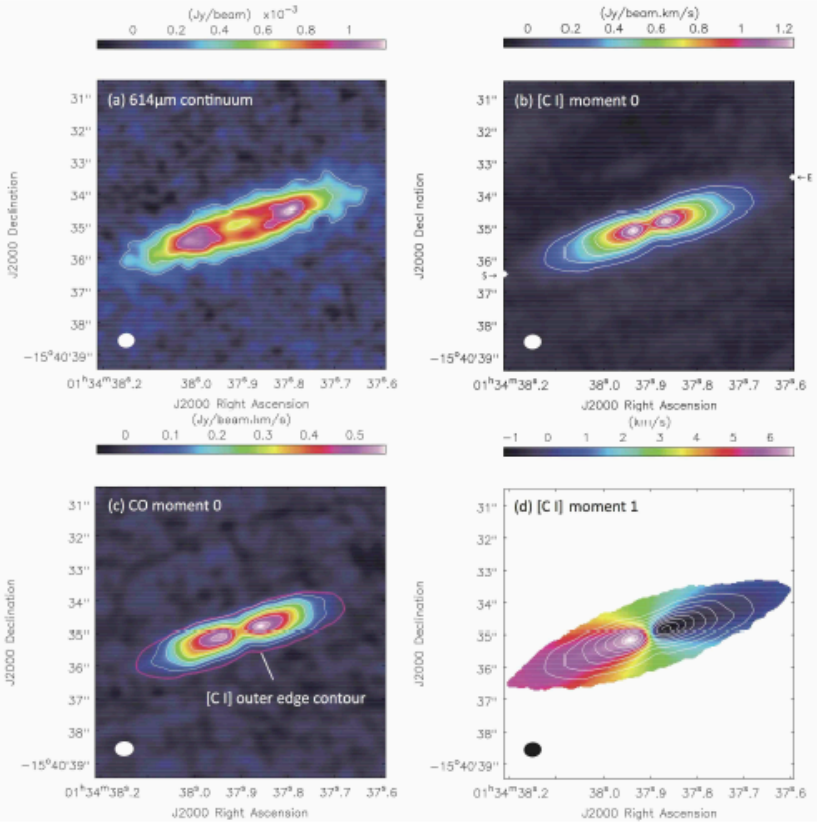

非常に強いCI emissionが観測され、大まかにはダストやCOと同じようなリング状の分布であった。

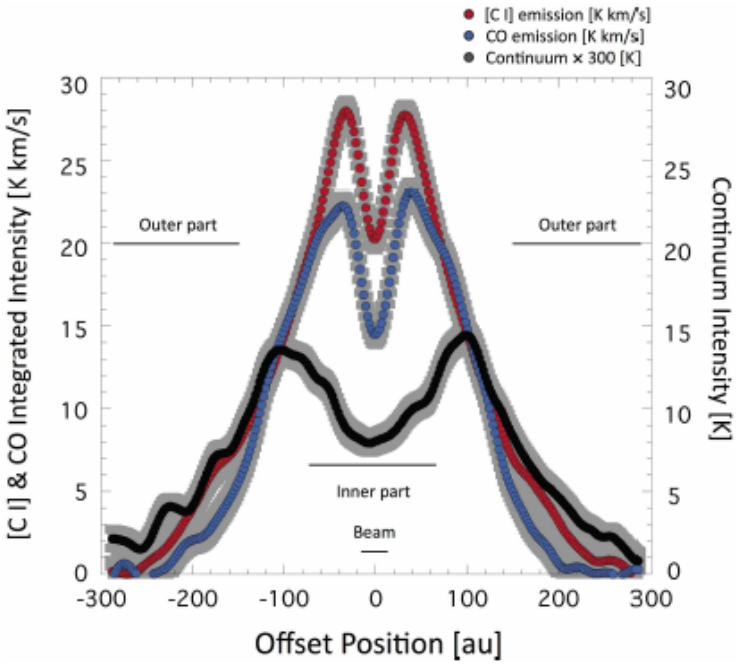

Fig. 3長軸方向のCI, CO, ダスト強度分布

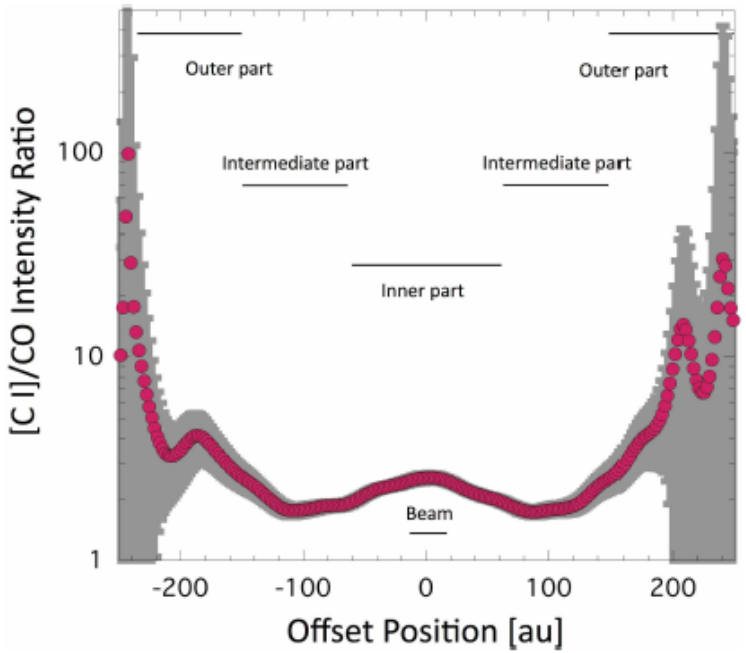

Fig. 4長軸方向のCI/CO比分布

わずかに円盤外縁部(r ~ 200au)付近で、CIとCOの空間分布が異なっており、CI/CO比で高くなっている。
=> 中心星の影響とは考えにくく、おそらく外部からの星間UV放射が円盤のCOを乖離していると思われる

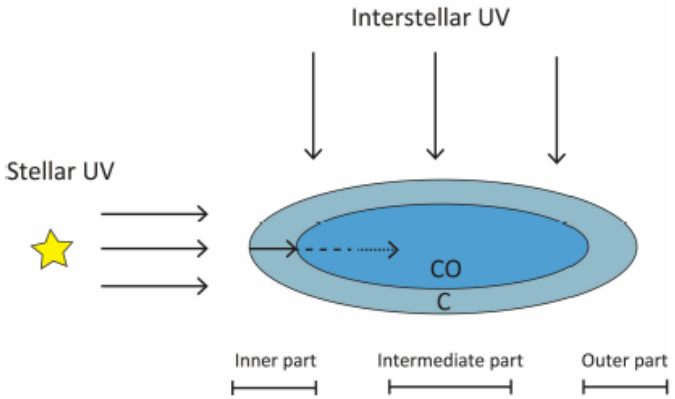

Measuring the magnetic field of young stars using iSHELL observations: BP Tau and V347 Aur

C. Flores,[1] M. S. Connelley,[1] B. Reipurth,[1] and A. Boogert[2]

[1] *Institute for Astronomy, University of Hawaii at Manoa, 640 N. Aohoku Place, Hilo, HI 96720, USA*
[2] *Institute for Astronomy, University of Hawaii at Manoa, 2680 Woodlawn Drive, Honolulu, HI 96822, USA*

(Received 2019 February 4; Revised 2019 July 22; Accepted 2019 July 24)

Submitted to ApJ

ABSTRACT

While it has been suggested that there is a connection between the magnetic properties and the internal structure of young stars, there have not been enough magnetic measurements to firmly establish such a correlation at the earliest ages. Here, we contribute to this endeavor by presenting stellar parameters and magnetic field strength measurements of BP Tau and V347 Aur, both stars observed with the near-infrared spectrograph iSHELL. We first test the accuracy of our method by fitting synthetic stellar spectra to a sample of nine main and post-main-sequence stars. We report uncertainties of $\sigma_{\rm Teff} = 91$ K in temperature and $\sigma_{\rm log(g)} = 0.14$ in gravity. We then apply the modeling technique to BP Tau and measure a surface magnetic field strength of $\langle B \rangle = 2.5^{+0.15}_{-0.16}$ kG, confirming literature results. For this star, however, we obtain a much lower temperature value than previous optical studies ($\Delta T \sim 400$ K) and interpret this significant temperature difference as due to the relatively higher impact of starspots at near-infrared wavelengths than at optical wavelengths. We further apply this technique to the class I protostellar source V347 Aur and measure for the first time its magnetic field strength $\langle B \rangle = 1.36^{+0.06}_{-0.05}$ kG and its surface gravity $\log(g) = 3.25^{+0.14}_{-0.14}$. Lastly, we combine our measurements with pre-main-sequence stellar evolutionary models and illustrate the effects produced by starspots on the retrieved masses and ages of young stars.

Origin of the PN molecule in star-forming regions: the enlarged sample

F. Fontani[1],* V.M. Rivilla[1], F.F.S. van der Tak[2,3], C. Mininni[1,4], M.T. Beltrán[1], and P. Caselli[5]

[1] *INAF-Osservatorio Astrofisico di Arcetri, Largo E. Fermi 5, I-50125, Florence, Italy*
[2] *SRON Netherlands Institute for Space Research, Landleven 12, 9747 AD Groningen, The Netherlands*
[3] *Kapteyn Astronomical Institute, University of Groningen, The Netherlands*
[4] *Dipartimento di Fisica e Astronomia, Università degli Studi di Firenze, I-50125 Florence, Italy*
[5] *Centre for Astrochemical Studies, Max-Planck-Institute for Extraterrestrial Physics, Giessenbachstrasse 1, 85748 Garching, Germany*

Accepted XXX. Received YYY; in original form ZZZ

ABSTRACT

Phosphorus nitride (PN) is the P-bearing species with the highest number of detections in star-forming regions. Multi-line studies of the molecule have shown that the excitation temperature of PN is usually lower than the gas kinetic temperature, suggesting that PN is likely in conditions of sub-thermal excitation. We present an analysis of PN which takes the possible sub-thermal excitation conditions into account in a sample of 24 massive star-forming regions. We observed PN (2–1), (3–2), (4–3), and (6–5) with the IRAM-30m and APEX telescopes and detected PN lines in 15 of them. Together with 9 similar sources detected in PN in previous works, we have analysed the largest sample of star-forming regions to date, made of 33 sources with 24 detections in total (among which 13 are new detections). Hence, we have increased the number of star-forming regions detected in PN by more than a factor 2. Our analysis indicates that the PN lines are indeed sub-thermally excited, but well described by a single excitation temperature. We have compared line profiles and fractional abundances of PN and SiO, a typical shock tracer, and found that almost all objects detected in PN have high-velocity SiO wings. Moreover, the SiO and PN abundances with respect to H_2 are correlated over several orders of magnitude, and uncorrelated with gas temperature. This clearly shows that the production of PN is strongly linked to the presence of shocked gas, and rules out alternative scenarios based on thermal evaporation from iced grain mantles.

Key words: Stars: formation – ISM: clouds – ISM: molecules – Radio lines: ISM

H_2 Ortho-Para Spin Conversion on Inhomogeneous Grain Surfaces

Kenji Furuya,[1] Yuri Aikawa,[2] Tetsuya Hama,[3] and Naoki Watanabe[3]

[1] *Center for Computer Sciences, University of Tsukuba, 305-8577 Tsukuba, Japan*
[2] *Department of Astronomy, The University of Tokyo, Bunkyo-ku, Tokyo 113-0033, Japan*
[3] *Institute of Low Temperature Science, Hokkaido University, Sapporo, Hokkaido 0600819, Japan*

(Received; Revised; Accepted)

Submitted to ApJ

ABSTRACT

We investigate the evolution of the ortho-to-para ratio of overall (gas + ice) H_2 via the nuclear spin conversion on grain surfaces coated with water ice under physical conditions that are relevant to star- and planet-forming regions. We utilize the rate equation model that considers adsorption of gaseous H_2 on grain surfaces, which have a variety of binding sites with a different potential energy depth, thermal hopping, desorption, and the nuclear spin conversion of adsorbed H_2. It is found that the spin conversion efficiency depends on the H_2 gas density and the surface temperature. As a general trend, enhanced H_2 gas density reduces the efficiency, while the temperature dependence is not monotonic; there is a critical surface temperature at which the efficiency is the maximum. At low temperatures, the exchange of gaseous and icy H_2 is inefficient (i.e., adsorbed H_2 does not desorb and hinders another gaseous H_2 to be adsorbed), while at warm temperatures, the residence time of H_2 on surfaces is too short for the spin conversion. Additionally, the spin conversion becomes more efficient with lowering the activation barriers for thermal hopping. We discuss whether the spin conversion on surfaces can dominate over that in the gas-phase in star- and planet-forming regions. Finally, we establish a simple, but accurate way to implement the H_2 spin conversion on grain surfaces in existing gas-ice astrochemical models.

Linking planetesimal and dust content in protoplanetary disks via a local toy model

Konstantin Gerbig[1,2], Christian T. Lenz[1], and Hubert Klahr[1]

[1] Max Planck Institute for Astronomy, Königstuhl 17, 69117 Heidelberg, Germany, e-mail: gerbig@mpia.de
[2] Department of Astronomy and Astrophysics, University of California, Santa Cruz, CA 95064, USA

Received 15/02/2019 Accepted 30/07/2019

ABSTRACT

Context. If planetesimal formation is an efficient process, as suggested by several models involving gravitational collapse of pebble clouds, then, before long, a significant part of the primordial dust mass should be absorbed in many km sized objects. A good understanding of the total amount of solids in the disk around a young star is crucial for planet formation theory. But as the mass of particles above the mm size cannot be assessed observationally, one must ask how much mass is hidden in bigger objects.
Aims. We perform 0-d local simulations to study how the planetesimal to dust and pebble ratio is evolving in time and to develop an understanding of the potentially existing mass in planetesimals for a certain amount of dust and pebbles at a given disk age.
Methods. We perform a parameter study based on a model considering dust growth, planetesimal formation and collisional fragmentation of planetesimals, while neglecting radial transport processes.
Results. While at early times, dust is the dominant solid particle species, there is a phase during which planetesimals make up a significant portion of the total mass starting at approximately $10^4 - 10^6$ yr. The time of this phase and the maximal total planetesimal mass strongly depend on the distance to the star R, the initial disk mass, and the efficiency of planetesimal formation ϵ. Planetesimal collisions are more significant in more massive disks, leading to lower relative planetesimal fractions compared to less massive disks. After approximately 10^6 yr, our model predicts planetesimal collisions to dominate, which resupplies small particles.
Conclusions. In our model, planetesimals form fast and everywhere in the disk. For a given ϵ, we were able to relate the dust content and mass of a given disk to its planetesimal content, providing us with some helpful basic intuition about mass distribution of solids and its dependence on underlying physical processes.

Key words. accretion, accretion disks – protoplanetary disks – stars: circumstellar matter – planets and satellites: formation

CHONDRULE FORMATION BY THE JOVIAN SWEEPING SECULAR RESONANCE

Munan Gong (龚慕南)[1], Xiaochen Zheng (郑晓晨)[2], Douglas N.C. Lin (林潮)[2,3,4], Kedron Silsbee[1], Clement Baruteau[5], Shude Mao (毛淑德)[2]

Accepted by ApJ

ABSTRACT

Chondrules are silicate spheroids found in meteorites, serving as important fossil records of the early solar system. In order to form chondrules, chondrule precursors must be heated to temperatures much higher than the typical conditions in the current asteroid belt. One proposed mechanism for chondrule heating is the passage through bow shocks of highly eccentric planetesimals in the protoplanetary disk in the early solar system. However, it is difficult for planetesimals to gain and maintain such high eccentricities. In this paper, we present a new scenario in which planetesimals in the asteroid belt region are excited to high eccentricities by the Jovian sweeping secular resonance in a depleting disk, leading to efficient formation of chondrules. We study the orbital evolution of planetesimals in the disk using semi-analytic models and numerical simulations. We investigate the dependence of eccentricity excitation on the planetesimal's size as well as the physical environment, and calculate the probability for chondrule formation. We find that $50 - 2000$ km planetesimals can obtain eccentricities larger than 0.6 and cause effective chondrule heating. Most chondrules form in high velocity shocks, in low density gas, and in the inner disk. The fraction of chondrule precursors which become chondrules is about $4-9\%$ between $1.5-3$ AU. Our model implies that the disk depletion timescale is $\tau_{\rm dep} \approx 1$ Myr, comparable to the age spread of chondrules; and that Jupiter formed before chondrules, no more than 0.7 Myr after the formation of the CAIs.

Close-in giant-planet formation via in-situ gas accretion and their natal disk properties

Yasuhiro Hasegawa[1], Tze Yeung Mathew Yu,[2] and Bradley M. S. Hansen[2]

[1] Jet Propulsion Laboratory, California Institute of Technology, Pasadena, CA 91109, USA
e-mail: yasuhiro.hasegawa@jpl.nasa.gov
[2] Department of Physics & Astronomy, University of California Los Angeles, Los Angeles, CA 90095, USA

Received; accepted

ABSTRACT

Aims. The origin of close-in Jovian planets is still elusive. We examine the in-situ gas accretion scenario as a formation mechanism of these planets.
Methods. We reconstruct natal disk properties from the occurrence rate distribution of close-in giant planets, under the assumption that the occurrence rate may reflect the gas accretion efficiency onto cores of these planets.
Results. We find that the resulting gas surface density profile becomes an increasing function of the distance from the central star with some structure at $r \simeq 0.1$ au. This profile is quite different from the standard minimum-mass solar nebula model, while our profile leads to better reproduction of the population of observed close-in super-Earths based on previous studies. We compute the resulting magnetic field profiles and find that our profiles can be fitted by stellar dipole fields ($\propto r^{-3}$) in the vicinity of the central star and large-scale fields ($\propto r^{-2}$) at the inner disk regions, either if the isothermal assumption breaks down or if nonideal MHD effects become important. For both cases, the transition between these two profiles occurs at $r \simeq 0.1$ au, which corresponds to the period valley of giant exoplanets.
Conclusions. Our work provides an opportunity to test the in-situ gas accretion scenario against disk quantities, which may constrain the gas distribution of the minimum-mass *extra*solar nebula.

L1495 Revisited: A PPMAP View of a Star-Forming Filament

A. D. P. Howard,[1★] A. P. Whitworth,[1] K. A. Marsh,[3] S. D. Clarke,[2] M. J.Griffin[1]
M. W. L. Smith[1] and O. D. Lomax[4]

[1]*School of Physics and Astronomy, Cardiff University, 5 The Parade, Cardiff, CF24 3AA, UK*
[2]*I. Physikalisches Institut, Universität zu Köln, Zülpicher Str. 77, D-50937 Köln, Germany*
[3]*IPAC, Caltech, 1200E California Boulevard, Pasadena, CA 91125, USA*
[4]*ESTEC, Keplerlaan 1, 2201 AZ Noordwijk, Netherlands*

Accepted XXX. Received YYY; in original form ZZZ

ABSTRACT
We have analysed the *Herschel* and SCUBA-2 dust continuum observations of the main filament in the Taurus L1495 star forming region, using the Bayesian fitting procedure PPMAP. (i) If we construct an average profile along the whole length of the filament, it has FWHM $\simeq 0.087 \pm 0.003$ pc; , but the closeness to previous estimates is coincidental. (ii) If we analyse small local sections of the filament, the column-density profile approximates well to the form predicted for hydrostatic equilibrium of an isothermal cylinder. (iii) The ability of PPMAP to distinguish dust emitting at different temperatures, and thereby to discriminate between the warm outer layers of the filament and the cold inner layers near the spine, leads to a significant reduction in the surface-density, Σ, and hence in the line-density, μ. If we adopt the canonical value for the critical line-density at a gas-kinetic temperature of 10 K, $\mu_{\rm CRIT} \simeq 16\,{\rm M}_\odot\,{\rm pc}^{-1}$, the filament is on average trans-critical, with $\bar{\mu} \sim \mu_{\rm CRIT}$; local sections where $\mu > \mu_{\rm CRIT}$ tend to lie close to pre-stellar cores. (iv) The ability of PPMAP to distinguish different types of dust, i.e. dust characterised by different values of the emissivity index, β, reveals that the dust in the filament has a lower emissivity index, $\beta \lesssim 1.5$, than the dust outside the filament, $\beta \gtrsim 1.7$, implying that the physical conditions in the filament have effected a change in the properties of the dust.